Anisotropic Topological Anderson Transitions in Chiral Symmetry Classes

Zhenyu Xiao,[1] Kohei Kawabata,[2,3] Xunlong Luo,[4] Tomi Ohtsuki,[5] and Ryuichi Shindou[1,*]
[1]International Center for Quantum Materials, Peking University, Beijing 100871, China
[2]Department of Physics, Princeton University, Princeton, New Jersey 08544, USA
[3]Institute for Solid State Physics, University of Tokyo, Kashiwa, Chiba 277-8581, Japan
[4]Science and Technology on Surface Physics and Chemistry Laboratory, Mianyang 621907, China
[5]Physics Division, Sophia University, Chiyoda-ku, Tokyo 102-8554, Japan

(Received 17 November 2022; revised 23 February 2023; accepted 23 June 2023; published 1 August 2023)

We study quantum phase transitions of three-dimensional disordered systems in the chiral classes (AIII and BDI) with and without weak topological indices. We show that the systems with a nontrivial weak topological index universally exhibit an emergent thermodynamic phase where wave functions are delocalized along one spatial direction but exponentially localized in the other two spatial directions, which we call the quasilocalized phase. Our extensive numerical study clarifies that the critical exponent of the Anderson transition between the metallic and quasilocalized phases, as well as that between the quasilocalized and localized phases, are different from that with no weak topological index, signaling the new universality classes induced by topology. The quasilocalized phase and concomitant topological Anderson transition manifest themselves in the anisotropic transport phenomena of disordered weak topological insulators and nodal-line semimetals, which exhibit the metallic behavior in one direction but the insulating behavior in the other directions.

DOI: 10.1103/PhysRevLett.131.056301

Introduction.—The last decades have seen remarkable discoveries of topological materials [1–3]. The interplay of disorder and topology leads to new types of quantum phase transitions, including the quantum Hall plateau transitions [4–13]. The universality classes of the disorder-driven metal-insulator transitions, known as the Anderson transitions, are characterized by the critical exponents and scaling functions, which are commonly believed to be determined solely by symmetry and spatial dimensions [14]. Many theories investigated whether topology can change the universality classes of the Anderson transitions [15–34]. Still, the role of topology in the Anderson transitions has been elusive.

Prime examples of three-dimensional (3D) topological materials include nodal-line semimetals characterized by the weak topological invariant [42–45]. Several recent experiments realized nodal-line semimetals in solid states [46–48], as well as synthetic materials of ultracold atoms [49] and photonic [50,51] and phononic [52] systems. Despite the significant interest in the physics of nodal-line semimetals [53–57], their unique transport signatures have remained largely unexplored.

In this Letter, we elucidate that the weak topological indices induce a novel thermodynamic phase in 3D disordered systems, including topological nodal-line semimetals, in the chiral classes. There, 3D wave functions are delocalized along one spatial direction and exponentially localized along the other two spatial directions—quasilocalized phase [Fig. 1(a)]. From extensive numerical calculations, we evaluate correlation-length critical exponents of the Anderson transitions among the metallic, quasilocalized, and localized phases [Fig. 1(a)] and find that they are distinct from the critical exponent in topologically trivial systems [Fig. 1(b)], signaling new universality classes induced by the topological indices. Notably, our quasilocalized phase and concomitant topological Anderson transition are of direct experimental relevance in the anisotropic transport that exhibits the metallic behavior in one direction but the insulating behavior in the other directions. While such anisotropic transport has played an important role in condensed matter physics [58–65], our results provide its new universal

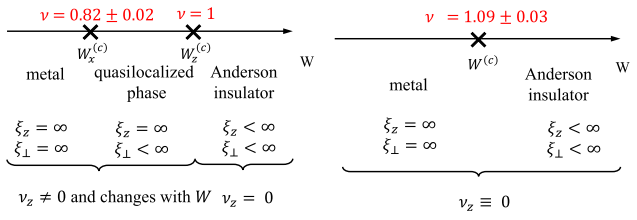

(a) topological models (b) nontopological models

FIG. 1. Phase diagrams of 3D disordered Hamiltonians in the chiral symmetry classes (a) with and (b) without the weak topological index ν_z. The critical exponents ν and localization lengths $\xi_z, \xi_\perp (\perp = x, y)$ along different directions are shown for different phases. The nontrivial critical exponents $\nu = 0.82 \pm 0.02$ and $\nu = 1.09 \pm 0.03$ are obtained for class BDI.

mechanism induced by the interplay of disorder and topology.

Lyapunov exponents and topological indices.—We study disorder-induced quantum phase transitions of 3D chiral-symmetric Hamiltonians $\mathcal{H}$. The localization properties along the μ direction ($\mu = x, y, z$) are efficiently captured by the Lyapunov exponents (LEs) along the μ direction in the limit $L \to \infty$, which are eigenvalues of [66,67]

$$\lim_{L_\mu \to \infty} \log (M^\dagger M)^{\frac{1}{2L_\mu}}. \tag{1}$$

Here, $M \equiv M_{L_\mu} M_{L_\mu - 1} \cdots M_1$ is the product of transfer matrices along the μ direction. The smallest positive LE gives the inverse of the localization length along the μ direction [68]. In the limit $L \to \infty$, the LEs of $\mathcal{H}$ form several continuous spectra [69]. If the spectra do not include zero, the wave function is localized along the μ direction. By contrast, if the spectra include zero, the localization length diverges, which means the delocalization of the wave function. The finite (infinite) localization length leads to the vanishing (nonvanishing) conductance in the same direction, as shown in the Supplemental Material [34].

Symmetries of Hamiltonians give constraints on the spectrum of the LEs. For example, because of the Hermiticity of $\mathcal{H}$, the LEs come in opposite-sign pairs. Moreover, in the presence of chiral symmetry, $\mathcal{H}$ can be brought into the block off diagonal structure,

$$\mathcal{H} = \begin{pmatrix} 0 & h \\ h^\dagger & 0 \end{pmatrix}, \tag{2}$$

where the off diagonal part h is assumed to be a square matrix. Because of chiral symmetry, the LEs of $\mathcal{H}$ reduce to the LEs of h and $h^\dagger$, which come in opposite-sign pairs, as shown in the Supplemental Material [34]. Consequently, we only need to calculate the product of the transfer matrices of h.

We demonstrate that a weak topological index ν_μ imposes another constraint on the spectrum of the LEs and plays a vital role in the emergence of the quasilocalized phase in disordered chiral-symmetric systems. To introduce ν_μ along the μ direction in the presence of disorder, let us insert a magnetic flux ϕ_μ through a closed loop along the μ direction. Then, the weak topological index ν_μ is given by the winding of $\det h(\phi_\mu)$ in Eq. (2) under an adiabatic insertion of a unit flux [70–72]:

$$\nu_\mu \equiv \frac{\mathrm{i}}{L^2} \int_0^{2\pi} \frac{d\phi_\mu}{2\pi} \partial_{\phi_\mu} \mathrm{Tr}\{\log[h(\phi_\mu)]\}, \tag{3}$$

where L^2 is the system size within the two directions perpendicular to the μ direction. Here, ν_μ is not necessarily quantized and takes an arbitrary real number. Notably, the weak topological index ν_μ and LEs of h are related to each other by [34,73]

$$\nu_\mu = \frac{1}{2L^2}(N_{+,\mu} - N_{-,\mu}), \tag{4}$$

where $N_{+,\mu}$ and $N_{-,\mu}$ are the numbers of positive and negative LEs of h along the μ direction, respectively.

Suppose $\mathcal{H}$ has a mobility gap around $E = 0$ and its zero-energy state is characterized by the weak topological indices $\nu_x = \nu_y = 0$, $\nu_z = 1$. From Eq. (4), a finite gap exists between the smallest positive LE and the largest negative LE such that $N_{+,z} - N_{-,z} = 2L^2$. By contrast, when disorder is strong enough, the zero-energy state is in a topologically trivial localized phase with $N_{+,z} = N_{-,z}$. Between the two localized phases, L^2 positive LEs of h cross zero, and ν_z continuously changes from 1 to 0 with respect to the disorder strength, where the localization length ξ_z along the z direction always diverges. Within this finite range with divergent ξ_z, the zero-energy state undergoes the Anderson transitions along the x and y directions, and thus a quasilocalized phase with divergent ξ_z and finite ξ_x and ξ_y emerges. Below, we clarify its nature, obtain the critical exponents of the Anderson transitions among the metallic, quasilocalized, and localized phases, and demonstrate the existence of new universality classes.

Model.—As a prototypical example, we study a two-orbital tight-binding model on a 3D cubic lattice [57]:

$$\mathcal{H} = \sum_{\boldsymbol{r}=(r_x,r_y,r_z)} \Big\{ \epsilon_{\boldsymbol{r}} c_{\boldsymbol{r}}^\dagger \sigma_z c_{\boldsymbol{r}} + \Big[\sum_{\mu=x,y} (t_\perp c_{\boldsymbol{r}+\boldsymbol{e}_\mu}^\dagger \sigma_z c_{\boldsymbol{r}}) - \mathrm{i} t_\parallel c_{\boldsymbol{r}+\boldsymbol{e}_z}^\dagger \sigma_y c_{\boldsymbol{r}} + t_\parallel' c_{\boldsymbol{r}+\boldsymbol{e}_z}^\dagger \sigma_z c_{\boldsymbol{r}} + \mathrm{H.c.} \Big] \Big\}. \tag{5}$$

Here, $c_{\boldsymbol{r}}$ is a two-component annihilation operator at the cubic lattice site $\boldsymbol{r}$, σ_μ ($\mu = x, y, z$) are Pauli matrices, $t_\perp$, $t_\parallel$, $t_\parallel'$ are real-valued parameters, and $\epsilon_{\boldsymbol{r}}$ is a random potential that distributes uniformly in $[-W/2, W/2]$. We assume $t_\perp, t_\parallel > 0$ for simplicity. This Hamiltonian respects time-reversal symmetry $\mathcal{H} = \mathcal{H}^*$ and chiral symmetry $\mathcal{H} = -\sigma_x \mathcal{H} \sigma_x$, and hence belongs to class BDI [3,14,74]. In addition, the ensemble of Hamiltonians is statistically invariant under the combination of time reversal and reflection with respect to the xy plane, which requires $N_{+,x} = N_{-,x}$, $N_{+,y} = N_{-,y}$ and $\nu_x = \nu_y = 0$, as shown in the Supplemental Material [34], while ν_z can be nonzero. In the clean limit, the Hamiltonian has an energy gap around $E = 0$ with $\nu_z = 1$ for $4t_\perp < 2|t_\parallel'|$. For $4t_\perp > 2|t_\parallel'|$, by contrast, the zero-energy state forms a nodal line in momentum space, resulting in $0 < \nu_z < 1$. In the following, we focus on the nodal-line-semimetal phase for $t_\parallel = t_\parallel' = 1/2$, $t_\perp = 1$ and study the Anderson transitions of the zero modes along all the directions. Still, we

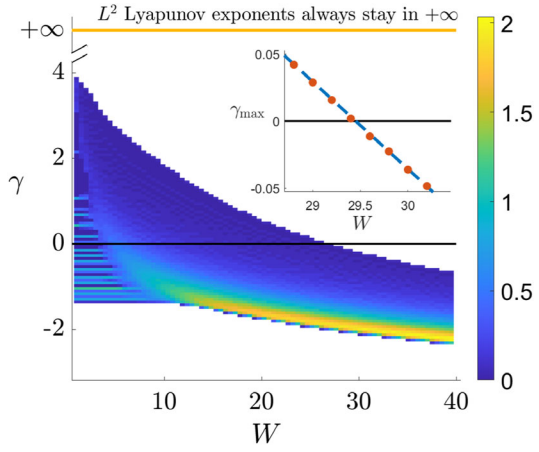

FIG. 2. $2L^2$ Lyapunov exponents (LEs) of the right-upper part h of the 3D nodal-line-semimetal model $\mathcal{H}$ along the z direction with the quasi-1D geometry $L \times L \times L_z$ ($L = 18$, $L_z = 2 \times 10^6$), plotted as a function of the disorder strength W. The color scale stands for the density $\rho(\gamma)$ of the LEs with the normalization $\int \rho(\gamma) d\gamma = 1$. The LEs of $\mathcal{H}$ are composed of the LEs of h and $h^\dagger$. Inset: the largest LE $\gamma_{\max}(W, L)$ among the smaller L^2 LEs as a function of W in the limit $L \to \infty$, obtained by a finite-size scaling fit. The error bars are smaller than the marks. The plot crosses zero linearly at $W_c^{(z)} = 29.45 \pm 0.05$; $\xi_z \sim (W - W_c^{(z)})^{-\nu'}$ with $\nu' = 1$ for $W > W_c^{(z)}$.

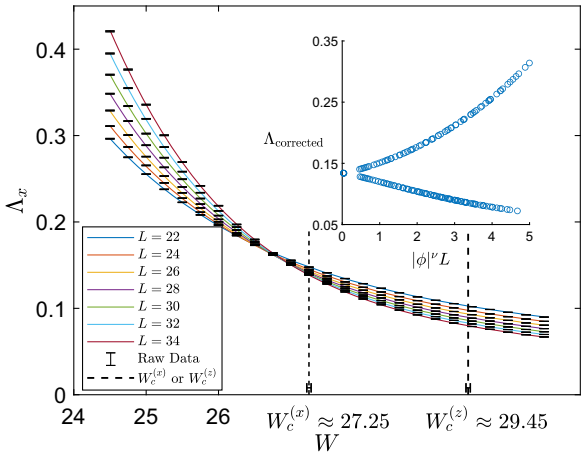

FIG. 3. Normalized localization length $\Lambda_x \equiv \xi_x/L$ along the x direction as a function of the disorder strength W in the nodal-line-semimetal model in Eq. (5) with the quasi-1D geometry $L \times L \times L_x$. The black points are the raw data with the error bars. The solid lines for different L and the dashed vertical line $W_c^{(x)}$ with the error bars are the results of the fitting according to Eq. (7) with $n = 3$. The dashed line $W_c^{(z)}$ is evaluated by the fitting of the Lyapunov exponent along the z direction by Eq. (6). Inset: single-parameter scaling function of Λ_x. $\Lambda_{\text{corrected}}$ is Λ_x subtracted by a contribution of the irrelevant scaling variable c in Eq. (7), and ϕ is the relevant scaling variable.

stress that the weak topological invariant ν_μ, rather than a nodal line itself, is the main ingredient for the quasilocalized phase.

Localization length ξ_z.—Figure 2 shows the distribution of LEs γ of h in Eq. (2) for the nodal-line-semimetal model $\mathcal{H}$ in Eq. (5) along the z direction in the quasi-1D geometry $L \times L \times L_z$. The distribution consists of two separate spectra, each of which contains L^2 LEs. The upper spectrum is always $\gamma = +\infty$ [34] and irrelevant to the Anderson transitions. For $W \le W_c^{(z)} \approx 29$, the lower spectrum includes zero $\gamma = 0$. Every positive LE in the lower spectrum for $W < W_c^{(z)}$ crosses zero when we increase W. At each crossing point, $N_{-,z}$ changes by 1. For $L \to \infty$, the crossing points become dense, and $\nu_z = 1 - N_{-,z}/L^2$ changes continuously with W. For $W > W_c^{(z)}$, all the LEs in the lower spectrum are negative (i.e., $N_{-,z} = L^2$), and the system is in a localized phase with no weak topological index $\nu_z = 0$. At $W = W_c^{(z)}$, the maximal LE in the lower spectrum crosses zero. Notably, $W_c^{(z)}$ for $L \to \infty$ cannot be determined by fitting ξ_z/L with a standard scaling function [e.g., see Eq. (7)] because ξ_z with finite L diverges at some $W < W_c^{(z)}$. Instead, we map the non-Hermitian matrix h into a well-localized Hermitian matrix by a similarity transformation [34,75], where the localization length obeys a scaling form in the strong disorder limit [76]. Then, we obtain the scaling form of the largest LE $\gamma_{\max}(W, L)$,

$$\gamma_{\max}(W, L) = a/L + \gamma_{\max}(W, L = \infty). \tag{6}$$

We numerically verify this scaling and determine the critical disorder strength $W_c^{(z)} = 29.45 \pm 0.05$ (inset of Fig. 2).

Localization length ξ_x, ξ_y.—The statistical symmetries mentioned above require LEs of h along the x and y directions to come in opposite-sign pairs. Thus, the localization length ξ_x along the x direction is always finite in the quasi-1D geometry with finite L. As shown in Fig. 3, the normalized localization length $\Lambda_x(W, L) \equiv \xi_x(W, L)/L$ shows scale-invariant behavior at a certain disorder strength $W_c^{(x)}$ well below $W = W_c^{(z)}$, indicating a quantum phase transition at $W = W_c^{(x)} < W_c^{(z)}$. To determine $W_c^{(x)}$ and the critical exponent ν, we use a finite-size scaling function and its polynomial expansion [68,77]. The scaling function for $\Lambda_x(W, L)$ is Taylor expanded with respect to the relevant scaling variable $\phi(w)$ and the least irrelevant scaling variable c up to the nth order and first order, respectively,

$$\Lambda_x(W, L) = \sum_{i=0}^{n} \sum_{j=0}^{1} a_{i,j} (\phi(w) L^{1/\nu})^i (c L^{-y})^j, \tag{7}$$

with $w \equiv (W - W_c^{(x)})/W_c^{(x)}$ and the scaling dimension $-y$ (< 0) of the least irrelevant scaling variable around a saddle-point fixed point. The fitting is carried out by the

TABLE I. Critical disorder strength $W_c^{(\mu)}$ and critical exponent ν for the 3D chiral classes, obtained by the polynomial fitting of the normalized localization length $\Lambda_\mu \equiv \xi_\mu/L$ along the μ direction ($\mu = x, y, z$) around critical points of different models with the quasi-one-dimensional geometry $L \times L \times L_\mu$. In the column "Topo," "✓" shows the nonzero weak topological index ν_z around the critical point, and "✗" shows zero topological indices in all the directions. The square brackets denote the 95% confidence interval.

Class	Topo	μ	$W_c^{(\mu)}$	ν
BDI	✓	x	27.241[27.194,27.303]	0.820[0.783,0.846]
AIII	✓	x	9.143[9.125,9.168]	0.824[0.776,0.862]
BDI	✗	z	23.220[23.167,23.293]	1.089[1.005,1.128]
BDI	✗	x	23.170[23.098,23.279]	1.042[0.943,1.099]
AIII	✗	z	8.091[8.074,8.096]	1.024[0.973,1.070]

χ^2 fitting method, and the confidence error bars for the optimal parameters are determined by the Monte Carlo method, as detailed in the Supplemental Material [34].

The first row in Table I shows the fitting results, where $W_c^{(x)} = 27.24 \pm 0.05$ is significantly smaller than $W_c^{(z)} = 29.45 \pm 0.05$, and the critical exponent at $W_c^{(x)}$ is evaluated as $\nu = 0.82 \pm 0.02$. The two different critical disorder strengths illustrate the emergence of the three distinct phases as a function of the disorder strength W [Fig. 1(a)]. For $W < W_c^{(x)}$, the localization lengths diverge along all directions (metallic phase). For $W > W_c^{(z)}$, the localization lengths are finite along all directions (Anderson insulator phase). For $W_c^{(x)} < W < W_c^{(z)}$, the localization lengths are finite along the x and y directions but diverge along the z direction (quasilocalized phase), and ν_z continuously changes as W changes. Our extensive numerical calculations show that the quasilocalized phase with divergent ξ_z but finite ξ_x, ξ_y universally appears between metallic and localized phases in different models with nonzero ν_z, as shown in the Supplemental Material [34]. The consistent critical exponent at $W = W_c^{(x)}$ was also obtained in Ref. [57], while a different critical exponent was obtained in Ref. [78] even in the same class. In this Letter, we elucidate that this difference originates from the emergence of the quasilocalized phase, which was not identified previously.

Quasilocalized phase.—Now, we clarify the nature of the quasilocalized phase induced by the weak topological index ν_μ. Let $\Phi(\boldsymbol{r}) = \langle \boldsymbol{r}|\Phi\rangle$ be a normalized wave function. The wavefunction interacts with an effective disorder potential $V_{\rm eff} = \langle\Phi|V|\Phi\rangle = \sum_{\boldsymbol{r}} V(\boldsymbol{r})|\Phi(\boldsymbol{r})|^2$, whose strength is given by $\langle V_{\rm eff}^2\rangle = W^2 P_2$ with the inverse participation ratio $P_2 \equiv \sum_{\boldsymbol{r}} |\Phi(\boldsymbol{r})|^4$. Here, $\langle\ldots\rangle$ denotes the disorder average: $\langle V(\boldsymbol{r})V(\boldsymbol{r}')\rangle = W^2\delta_{\boldsymbol{r},\boldsymbol{r}'}$. As long as W is finite, the following argument is applicable to general $V(\boldsymbol{r})$, including the box disorder in $[-W/2, W/2]$ used for the numerical calculations. Let us introduce the integrated weight of the wave function in the zth layer by $|\phi(z)|^2 = \sum_{x,y} |\Phi(\boldsymbol{r})|^2$ and also the one-dimensional inverse participation ratio $P_2^z \equiv \sum_z |\phi(z)|^4$. P_2^x, P_2^y can be defined in the same manner. P_2^μ measures the localization property of $\Phi(\boldsymbol{r})$ along the μ direction, giving an upper bound of P_2: $P_2 \le P_2^\mu (\mu = x, y, z)$ [34]. If the wave function is extended along the z direction (i.e., $P_2^z \sim L_z^{-1}$ [14]), P_2 and $\langle V_{\rm eff}^2\rangle$ should vanish for $L_z \to \infty$, and $\Phi(\boldsymbol{r})$ must be extended along all the directions. If P_2^z is finite even for $L_z \to \infty$, by contrast, P_2^x and P_2^y should also be finite for $L_x, L_y \to \infty$. Otherwise, $\Phi(\boldsymbol{r})$ is extended within all the directions, which contradicts finite P_2^z. In the intermediate phase discussed above, we find that ξ_x is finite, but ξ_z diverges. While finite ξ_x means finite P_2 and P_2^z, divergent ξ_z with finite P_2^z means that the wave function $\Phi(\boldsymbol{r})$ must be quasilocalized along the z direction. Thus, the wave function in the intermediate phase is localized within the xy plane and delocalized only along the z direction—quasilocalized phase. Here, $\Phi(\boldsymbol{r})$ along the z direction shares the same localization properties as wave functions of 1D chiral-symmetric systems at a topological phase transition, where the 1D topological index changes [14,70,71,79–81]. The 3D system in the intermediate phase is effectively decoupled into 1D wires because of finite $\xi_{x,y}$.

The emergence of the quasilocalized phase in 3D systems is a consequence of finite $P_2^{\rm 1D}$ at the topological phase transition of 1D chiral-symmetric systems. Generally, when a d'-dimensional wave function $\Phi(\boldsymbol{R})$ in $\boldsymbol{R} \equiv (\boldsymbol{r}, \boldsymbol{s})$ with $\boldsymbol{r} = (r_1, \ldots, r_d)$ and $\boldsymbol{s} = (s_1, \ldots, s_{d'-d})$ $(d < d')$ is made out of coupled d-dimensional wave functions $\psi(\boldsymbol{r})$ at a critical point, $\Phi(\boldsymbol{R})$ is more extended than $\psi(\boldsymbol{r})$ along the $\boldsymbol{r}$ direction because of the interlayer coupling, as shown in the Supplemental Material [34]. Thus, the effective disorder strength for the d'-dimensional wave function $\Phi(\boldsymbol{R})$ is bounded by the d-dimensional inverse participation ratio $P_2^{\psi(\boldsymbol{r})}$ of $\psi(\boldsymbol{r})$. When the wave function $\psi(\boldsymbol{r})$ has finite $P_2^{\psi(\boldsymbol{r})}$ at the critical point, the effective disorder strength can be finite, and $\Phi(\boldsymbol{R})$ can be either extended or localized within the $\boldsymbol{s}$ direction. On the other hand, when $P_2^{\psi(\boldsymbol{r})}$ is zero at the critical point, e.g., 2D critical wave functions at the quantum Hall plateau transition, the effective disorder strength is zero, and the d'-dimensional wave function should always be extended in both $\boldsymbol{r}$ and $\boldsymbol{s}$ directions. Notably, the 1D topological phase transitions in all the three chiral classes are characterized by finite P_2 [14]. In the following, we demonstrate the quasilocalized phases also in the 3D chiral unitary class, which is consistent with the above argument.

Model without time-reversal symmetry.—We add a time-reversal-breaking but chiral-symmetric disorder $\Delta\mathcal{H}$ to the model $\mathcal{H}$ in Eq. (5):

$$\mathcal{H}_1 = \mathcal{H} + \Delta\mathcal{H}, \qquad \Delta\mathcal{H} = \sum_{\boldsymbol{r}} \epsilon'_{\boldsymbol{r}} c^\dagger_{\boldsymbol{r}} \sigma_y c_{\boldsymbol{r}}, \tag{8}$$

with the random potential $\epsilon'_{\boldsymbol{r}}$, where $(\epsilon_{\boldsymbol{r}}, \epsilon'_{\boldsymbol{r}}) = (V_{\boldsymbol{r}} \cos\theta_{\boldsymbol{r}}, V_{\boldsymbol{r}} \sin\theta_{\boldsymbol{r}})$, and $\theta_{\boldsymbol{r}}$ and $V_{\boldsymbol{r}}$ distribute uniformly in the range of $[0, 2\pi)$ and $[0, W]$, respectively. This model only respects chiral symmetry and belongs to class AIII, in which the weak topological indices are defined in the same manner. It shows a similar phase diagram as in the previous model in class BDI with $W_c^{(z)} = 9.8 \pm 0.1$ and $W_c^{(x)} = 9.14 \pm 0.01$ (see Fig. 1 and Table I). The critical exponents are the same as those in the models in class BDI, which suggests possible superuniversality in 3D systems in the chiral classes with the topological indices.

Models with trivial topological indices.—To further clarify the role of the topological indices, we also study a topologically trivial model in class BDI with statistical symmetries. The statistical symmetry of time reversal combined with reflection with respect to the xz or yz plane makes all three topological indices vanish, as shown in the Supplemental Material [34]. In addition, LEs of h along any direction come in opposite-sign pairs, and the localization lengths along the x and y directions are the same. On increasing the disorder strength, the model undergoes the Anderson transition, where the normalized localization lengths Λ_x and Λ_z along the x and z directions both show scale-invariant behaviors. The critical disorder strengths and critical exponents determined from Λ_x and Λ_z are consistent with each other (see Table I), which suggests that the scale-invariant behavior of Λ_x and Λ_z comes from the same quantum phase transition [Fig. 1(b)]. The evaluated critical exponent $\nu = 1.089[1.005, 1.128]$ is different from ν at $W = W_c^{(x)}$ of the topological model, and consistent with ν of the topologically trivial models in Ref. [78]. We also evaluate the critical exponent in the chiral unitary class without weak topological indices as $\nu = 1.024[0.973, 1.070]$ (Table I), which is different from ν of the topological models in the same symmetry class and consistent with Refs. [33,78].

Summary and discussion.—In this Letter, we show that in 3D systems in the chiral classes, the weak topological indices induce a disorder-driven quasilocalized phase where wave functions are delocalized only along one direction and localized along the other two directions. The critical exponents of the Anderson transitions among metal, quasilocalized, and localized phases are all different (Fig. 1). We believe that these conclusions hold also in the chiral symplectic class (class CII). Our quasilocalized phase leads to the anisotropic transport phenomena of topological nodal-line semimetals [43–52], where the conductance along the direction with the divergent localization length takes finite values with larger fluctuations, while it vanishes along the other directions in the thermodynamic limit, as shown in the Supplemental Material [34]. The quasilocalized phase may potentially find practical applications such as quantum devices that control the direction of currents.

Our results are also relevant to non-Hermitian physics [82–84], where the interplay between disorder and dissipation has recently acquired renewed interest. In fact, all the disorder-driven phases and phase transitions in this Letter are characterized by the LEs of the off diagonal part h in Eq. (2), which can be considered as a non-Hermitian Hamiltonian [33]. Anisotropy of $\mathcal{H}$ corresponds to nonreciprocity of h and leads to transport phenomena unique to open systems.

3D chiral-symmetric systems also host a strong topological index [1–3]. By a similar numerical study, we find that the strong index does not lead to the quasilocalized phases, not influencing the universality classes of the Anderson transitions [85]. It also remains to be explored whether the quasilocalized phase appears and whether the topological indices change the universality classes of the Anderson transitions in 2D systems, as well as nodal-line semimetals protected by spatial symmetry.

Z. X. thanks Zhida Song, Lingxian Kong, and Yeyang Zhang for fruitful discussions. Z. X. and R. S. were supported by the National Basic Research Programs of China (No. 2019YFA0308401) and by National Natural Science Foundation of China (No. 11674011 and No. 12074008). K. K. was supported by JSPS Overseas Research Fellowship, and Grant No. GBMF8685 from the Gordon and Betty Moore Foundation toward the Princeton theory program. X. L. was supported by the National Natural Science Foundation of China, Grant No. 12105253. T. O. was supported by JSPS KAKENHI Grants No. 19H00658 and No. 22H05114.

*rshindou@pku.edu.cn

[1] M. Z. Hasan and C. L. Kane, Colloquium: Topological insulators, Rev. Mod. Phys. **82**, 3045 (2010).
[2] X.-L. Qi and S.-C. Zhang, Topological insulators and superconductors, Rev. Mod. Phys. **83**, 1057 (2011).
[3] C.-K. Chiu, J. C. Y. Teo, A. P. Schnyder, and S. Ryu, Classification of topological quantum matter with symmetries, Rev. Mod. Phys. **88**, 035005 (2016).
[4] K. v. Klitzing, G. Dorda, and M. Pepper, New Method for High-Accuracy Determination of the Fine-Structure Constant Based on Quantized Hall Resistance, Phys. Rev. Lett. **45**, 494 (1980).
[5] J. Chalker and P. Coddington, Percolation, quantum tunnelling and the integer Hall effect, J. Phys. C **21**, 2665 (1988).
[6] A. M. M. Pruisken, Universal Singularities in the Integral Quantum Hall Effect, Phys. Rev. Lett. **61**, 1297 (1988).
[7] B. Huckestein, Scaling theory of the integer quantum Hall effect, Rev. Mod. Phys. **67**, 357 (1995).
[8] M. J. Bhaseen, I. I. Kogan, O. A. Soloviev, N. Taniguchi, and A. M. Tsvelik, Towards a field theory of the plateau transitions in the integer quantum Hall effect, Nucl. Phys. B **580**, 688 (2000).

[9] K. Slevin and T. Ohtsuki, Critical exponent for the quantum Hall transition, Phys. Rev. B **80**, 041304(R) (2009).

[10] E. Prodan, T. L. Hughes, and B. A. Bernevig, Entanglement Spectrum of a Disordered Topological Chern Insulator, Phys. Rev. Lett. **105**, 115501 (2010).

[11] Q. Zhu, P. Wu, R. N. Bhatt, and X. Wan, Localization-length exponent in two models of quantum Hall plateau transitions, Phys. Rev. B **99**, 024205 (2019).

[12] M. Puschmann, P. Cain, M. Schreiber, and T. Vojta, Integer quantum Hall transition on a tight-binding lattice, Phys. Rev. B **99**, 121301(R) (2019).

[13] E. J. Dresselhaus, B. Sbierski, and I. A. Gruzberg, Scaling Collapse of Longitudinal Conductance near the Integer Quantum Hall Transition, Phys. Rev. Lett. **129**, 026801 (2022).

[14] F. Evers and A. D. Mirlin, Anderson transitions, Rev. Mod. Phys. **80**, 1355 (2008).

[15] Y. Asada, K. Slevin, and T. Ohtsuki, Anderson Transition in Two-Dimensional Systems with Spin-Orbit Coupling, Phys. Rev. Lett. **89**, 256601 (2002).

[16] Y. Asada, K. Slevin, and T. Ohtsuki, Anderson transition in the three dimensional symplectic universality class, J. Phys. Soc. Jpn. **74**, 238 (2005).

[17] M. Onoda, Y. Avishai, and N. Nagaosa, Localization in a Quantum Spin Hall System, Phys. Rev. Lett. **98**, 076802 (2007).

[18] H. Obuse, A. Furusaki, S. Ryu, and C. Mudry, Two-dimensional spin-filtered chiral network model for the $\mathbb{Z}_2$ quantum spin-Hall effect, Phys. Rev. B **76**, 075301 (2007).

[19] S. Ryu, C. Mudry, H. Obuse, and A. Furusaki, $\mathbb{Z}_2$ Topological Term, the Global Anomaly, and the Two-Dimensional Symplectic Symmetry Class of Anderson Localization, Phys. Rev. Lett. **99**, 116601 (2007).

[20] K. Nomura, M. Koshino, and S. Ryu, Topological Delocalization of Two-Dimensional Massless Dirac Fermions, Phys. Rev. Lett. **99**, 146806 (2007).

[21] A. D. Mirlin, F. Evers, I. V. Gornyi, and P. M. Ostrovsky, Anderson transitions: Criticality, symmetries, and topologies, Int. J. Mod. Phys. B **24**, 1577 (2010).

[22] E. J. König, P. M. Ostrovsky, I. V. Protopopov, and A. D. Mirlin, Metal-insulator transition in two-dimensional random fermion systems of chiral symmetry classes, Phys. Rev. B **85**, 195130 (2012).

[23] Z. Ringel, Y. E. Kraus, and A. Stern, Strong side of weak topological insulators, Phys. Rev. B **86**, 045102 (2012).

[24] L. Fu and C. L. Kane, Topology, Delocalization via Average Symmetry and the Symplectic Anderson Transition, Phys. Rev. Lett. **109**, 246605 (2012).

[25] K. Slevin and T. Ohtsuki, Estimate of the critical exponent of the Anderson transition in the three and four-dimensional unitary universality classes, J. Phys. Soc. Jpn. **85**, 104712 (2016).

[26] B. Roy, Y. Alavirad, and J. D. Sau, Global Phase Diagram of a Three-Dimensional Dirty Topological Superconductor, Phys. Rev. Lett. **118**, 227002 (2017).

[27] X. Luo, B. Xu, T. Ohtsuki, and R. Shindou, Quantum multicriticality in disordered Weyl semimetals, Phys. Rev. B **97**, 045129 (2018).

[28] N. Yoshioka, Y. Akagi, and H. Katsura, Learning disordered topological phases by statistical recovery of symmetry, Phys. Rev. B **97**, 205110 (2018).

[29] Z.-D. Song, B. Lian, R. Queiroz, R. Ilan, B. A. Bernevig, and A. Stern, Delocalization Transition of a Disordered Axion Insulator, Phys. Rev. Lett. **127**, 016602 (2021).

[30] J. H. Son and S. Raghu, Three-dimensional network model for strong topological insulator transitions, Phys. Rev. B **104**, 125142 (2021).

[31] Z. Pan, T. Wang, T. Ohtsuki, and R. Shindou, Renormalization group analysis of Dirac fermions with a random mass, Phys. Rev. B **104**, 174205 (2021).

[32] T. Wang, Z. Pan, T. Ohtsuki, I. A. Gruzberg, and R. Shindou, Multicriticality of two-dimensional class-D disordered topological superconductors, Phys. Rev. B **104**, 184201 (2021).

[33] X. Luo, Z. Xiao, K. Kawabata, T. Ohtsuki, and R. Shindou, Unifying the Anderson transitions in Hermitian and non-Hermitian systems, Phys. Rev. Res. **4**, L022035 (2022).

[34] See Supplemental Material at http://link.aps.org/supplemental/10.1103/PhysRevLett.131.056301 for summary of known critical exponents in topological insulators; inverse participation ratio; transfer matrix analyses; a relation between weak topological indices and Lyapunov exponents; statistical symmetry; details of finite-size scaling analyses; quasilocalized phase in other topological models; Anderson transition in nontopological models; and detailed numerical results of conductance in metal, quasilocalized, and Anderson localized phases, which includes Refs. [35–41].

[35] A. Crisanti, G. Paladin, and A. Vulpiani, *Products of Random Matrices* (Springer, Berlin, Heidelberg, 1993).

[36] K. Kawabata, K. Shiozaki, M. Ueda, and M. Sato, Symmetry and Topology in Non-Hermitian Physics, Phys. Rev. X **9**, 041015 (2019).

[37] I. Goldhirsch, P.-L. Sulem, and S. A. Orszag, Stability and Lyapunov stability of dynamical systems: A differential approach and a numerical method, Physica (Amsterdam) **27D**, 311 (1987).

[38] I. C. Fulga, A. R. Akhmerov, J. Tworzydło, B. Béri, and C. W. J. Beenakker, Thermal metal-insulator transition in a helical topological superconductor, Phys. Rev. B **86**, 054505 (2012).

[39] L. Fu, C. L. Kane, and E. J. Mele, Topological Insulators in Three Dimensions, Phys. Rev. Lett. **98**, 106803 (2007).

[40] J. B. Pendry, A. MacKinnon, and A. B. Pretre, Maximal fluctuations—A new phenomenon in disordered systems, Physica (Amsterdam) **168A**, 400 (1990).

[41] B. Kramer, T. Ohtsuki, and S. Kettemann, Random network models and quantum phase transitions in two dimensions, Phys. Rep. **417**, 211 (2005).

[42] A. A. Burkov, M. D. Hook, and L. Balents, Topological nodal semimetals, Phys. Rev. B **84**, 235126 (2011).

[43] A. P. Schnyder and P. M. R. Brydon, Topological surface states in nodal superconductors, J. Phys. Condens. Matter **27**, 243201 (2015).

[44] C. Fang, H. Weng, X. Dai, and Z. Fang, Topological nodal line semimetals, Chin. Phys. B **25**, 117106 (2016).

[45] N. P. Armitage, E. J. Mele, and A. Vishwanath, Weyl and Dirac semimetals in three-dimensional solids, Rev. Mod. Phys. **90**, 015001 (2018).

[46] G. Bian *et al.*, Topological nodal-line fermions in spin-orbit metal $PbTaSe_2$, Nat. Commun. **7**, 10556 (2016).

[47] L. M. Schoop, M. N. Ali, C. Straßer, A. Topp, A. Varykhalov, D. Marchenko, V. Duppel, S. S. P. Parkin, B. V. Lotsch, and C. R. Ast, Dirac cone protected by non-symmorphic symmetry and three-dimensional Dirac line node in ZrSiS, Nat. Commun. **7**, 11696 (2016).

[48] C. Chen, X.-T. Zeng, Z. Chen, Y. X. Zhao, X.-L. Sheng, and S. A. Yang, Second-Order Real Nodal-Line Semimetal in Three-Dimensional Graphdiyne, Phys. Rev. Lett. **128**, 026405 (2022).

[49] B. Song, C. He, S. Niu, L. Zhang, Z. Ren, X.-J. Liu, and G.-B. Jo, Observation of nodal-line semimetal with ultracold fermions in an optical lattice, Nat. Phys. **15**, 911 (2019).

[50] L. Xia, Q. Guo, B. Yang, J. Han, C.-X. Liu, W. Zhang, and S. Zhang, Observation of Hourglass Nodal Lines in Photonics, Phys. Rev. Lett. **122**, 103903 (2019).

[51] W. Gao, B. Yang, Biao Tremain, H. Liu, Q. Guo, L. Xia, A. P. Hibbins, and S. Zhang, Experimental observation of photonic nodal line degeneracies in metacrystals, Nat. Commun. **9**, 950 (2019).

[52] W. Deng, J. Lu, F. Li, X. Huang, M. Yan, J. Ma, and Z. Liu, Nodal rings and drumhead surface states in phononic crystals, Nat. Commun. **10**, 1769 (2019).

[53] R. Nandkishore, Weyl and Dirac loop superconductors, Phys. Rev. B **93**, 020506(R) (2016).

[54] S. Sur and R. Nandkishore, Instabilities of Weyl loop semimetals, New J. Phys. **18**, 115006 (2016).

[55] S. V. Syzranov and B. Skinner, Electron transport in nodal-line semimetals, Phys. Rev. B **96**, 161105(R) (2017).

[56] M. Gonçalves, P. Ribeiro, E. V. Castro, and M. A. N. Araújo, Disorder-Driven Multifractality Transition in Weyl Nodal Loops, Phys. Rev. Lett. **124**, 136405 (2020).

[57] X. Luo, B. Xu, T. Ohtsuki, and R. Shindou, Critical behavior of Anderson transitions in three-dimensional orthogonal classes with particle-hole symmetries, Phys. Rev. B **101**, 020202(R) (2020).

[58] M. J. Cohen, L. B. Coleman, A. F. Garito, and A. J. Heeger, Electrical conductivity of tetrathiofulvalinium tetracyanoquinodimethan (TTF)(TCNQ), Phys. Rev. B **10**, 1298 (1974).

[59] M. P. Lilly, K. B. Cooper, J. P. Eisenstein, L. N. Pfeiffer, and K. W. West, Evidence for an Anisotropic State of Two-Dimensional Electrons in High Landau Levels, Phys. Rev. Lett. **82**, 394 (1999).

[60] R. R. Du, D. C. Tsui, H. L. Stormer, L. N. Pfeiffer, K. W. Baldwin, and K. W. West, Strongly anisotropic transport in higher two-dimensional Landau levels, Solid State Commun. **109**, 389 (1999).

[61] Y. Ando, K. Segawa, S. Komiya, and A. N. Lavrov, Electrical Resistivity Anisotropy from Self-Organized One Dimensionality in High-Temperature Superconductors, Phys. Rev. Lett. **88**, 137005 (2002).

[62] R. A. Borzi, S. A. Grigera, J. Farrell, R. S. Perry, S. J. S. Lister, S. L. Lee, D. A. Tennant, Y. Maeno, and A. P. Mackenzie, Formation of a nematic fluid at high fields in $Sr_3Ru_2O_7$, Science **315**, 214 (2007).

[63] V. Hinkov, D. Haug, B. Fauqué, P. Bourges, Y. Sidis, A. Ivanov, C. Bernhard, C. T. Lin, and B. Keimer, Electronic liquid crystal state in the high-temperature superconductor $YBa_2Cu_3O_{6.45}$, Science **319**, 597 (2008).

[64] J.-H. Chu, J. G. Analytis, K. D. Greve, P. L. McMahon, Z. Islam, Y. Yamamoto, and I. R. Fisher, In-plane resistivity anisotropy in an underdoped iron arsenide superconductor, Science **329**, 824 (2010).

[65] E. Fradkin, S. A. Kivelson, M. J. Lawler, J. P. Eisenstein, and A. P. Mackenzie, Nematic Fermi fluids in condensed matter physics, Annu. Rev. Condens. Matter Phys. **1**, 153 (2010).

[66] A. MacKinnon and B. Kramer, One-Parameter Scaling of Localization Length and Conductance in Disordered Systems, Phys. Rev. Lett. **47**, 1546 (1981).

[67] A. MacKinnon and B. Kramer, The scaling theory of electrons in disordered solids: Additional numerical results, Z. Phys. B **53**, 1 (1983).

[68] K. Slevin and T. Ohtsuki, Critical exponent for the Anderson transition in the three-dimensional orthogonal universality class, New J. Phys. **16**, 015012 (2014).

[69] P. Markos, Phenomenological theory of the metal-insulator transition, J. Phys. Condens. Matter **7**, 8361 (1995).

[70] I. Mondragon-Shem, T. L. Hughes, J. Song, and E. Prodan, Topological Criticality in the Chiral-Symmetric AIII Class at Strong Disorder, Phys. Rev. Lett. **113**, 046802 (2014).

[71] A. Altland, D. Bagrets, L. Fritz, A. Kamenev, and H. Schmiedt, Quantum Criticality of Quasi-One-Dimensional Topological Anderson Insulators, Phys. Rev. Lett. **112**, 206602 (2014).

[72] J. Claes and T. L. Hughes, Disorder driven phase transitions in weak AIII topological insulators, Phys. Rev. B **101**, 224201 (2020).

[73] L. Molinari, Spectral duality and distribution of exponents for transfer matrices of block-tridiagonal Hamiltonians, J. Phys. A **36**, 4081 (2003).

[74] A. Altland and M. R. Zirnbauer, Nonstandard symmetry classes in mesoscopic normal-superconducting hybrid structures, Phys. Rev. B **55**, 1142 (1997).

[75] N. Hatano and D. R. Nelson, Localization Transitions in Non-Hermitian Quantum Mechanics, Phys. Rev. Lett. **77**, 570 (1996).

[76] Y. Asada, K. Slevin, and T. Ohtsuki, Numerical estimation of the β function in two-dimensional systems with spin-orbit coupling, Phys. Rev. B **70**, 035115 (2004).

[77] K. Slevin and T. Ohtsuki, Corrections to Scaling at the Anderson Transition, Phys. Rev. Lett. **82**, 382 (1999).

[78] T. Wang, T. Ohtsuki, and R. Shindou, Universality classes of the Anderson transition in the three-dimensional symmetry classes AIII, BDI, C, D, and CI, Phys. Rev. B **104**, 014206 (2021).

[79] L. Balents and M. P. A. Fisher, Delocalization transition via supersymmetry in one dimension, Phys. Rev. B **56**, 12970 (1997).

[80] H. Mathur, Feynman's propagator applied to network models of localization, Phys. Rev. B **56**, 15794 (1997).

[81] P. W. Brouwer, C. Mudry, B. D. Simons, and A. Altland, Delocalization in Coupled One-Dimensional Chains, Phys. Rev. Lett. **81**, 862 (1998).

[82] V. V. Konotop, J. Yang, and D. A. Zezyulin, Nonlinear waves in $\mathcal{PT}$-symmetric systems, Rev. Mod. Phys. **88**, 035002 (2016).

[83] L. Feng, R. El-Ganainy, and L. Ge, Non-Hermitian photonics based on parity-time symmetry, Nat. Photonics **11**, 752 (2017).

[84] R. El-Ganainy, K. G. Makris, M. Khajavikhan, Z. H. Musslimani, S. Rotter, and D. N. Christodoulides, Non-Hermitian physics and $\mathcal{PT}$ symmetry, Nat. Phys. **14**, 11 (2018).

[85] Z. Xiao, K. Kawabata, X. Luo, T. Ohtsuki, and R. Shindou, Unpublished.